SHARE

SEVENTH FRAMEWORK PROGRAMME

Grant Agreement no. 226967

SEISMIC HAZARD HARMONIZATION IN EUROPE

Project Acronym: SHARE

SP 1-Cooperation

Collaborative project: Small or medium-scale focused research project

THEME 6: Environment

Call: ENV.2008.1.3.1.1 Development of a common methodology and tools to evaluate earthquake hazard in Europe

D4.6– Non-linear site amplification factors for the next generation of European GMPEs

Due date of deliverable: 30.05.2011
Actual submission date: 28.06.2012

Start date of project: 2009-06-01 Duration: 36

Middle East Technical University (METU)
M. A. Sandikkaya, S. Akkar

Laboratoire de Geophysique Interne et Tectonophysique, Universite Joseph Fourier (LGIT-UJF)
P.-Y. Bard

Revision: 1

Dissemination Level		
PU	Public	x
PP	Restricted to other programme participants (including the Commission Services)	
RE	Restricted to a group specified by the consortium (including the Commission Services)	
CO	Confidential, only for members of the consortium (including the Commission Services)	

Note on Revision 1 of Deliverable 4.6

This deliverable has been submitted to the Bulletin of Seismological Society of America with the same title.

SHARE

SEISMIC HAZARD HARMONIZATION IN EUROPE

WP4: STRONG GROUND MOTION MODELLING

REPORT ON THE NONLINEAR SITE AMPLIFICATION MODEL FOR THE NEXT PAN-EUROPEAN GROUND-MOTION PREDICTION EQUATIONS

(submitted to BSSA for possible publication)

M.A. Sandıkkaya, S. Akkar and P-Y Bard

Earthquake Engineering Research Center, Middle East Technical University, 06800 Ankara, Turkey

Institut des Sciences de la Terre, 38041 Grenoble CEDEX 9, France

March, 2012

CONTENTS

INTRODUCTION

The recent trend in ground-motion prediction equations (GMPEs) is to represent the soil effects by a site amplification model that mimics the soil behavior through functional forms that are either based on the stochastic simulations or empirical data. The site conditions are generally described by the time-based average of the shear-wave velocity profile in the upper 30 m soil (V_{S30}) but some models also consider complementary parameters to this proxy to fully capture the genuine soil behavior under various circumstances (e.g., Z1.0 and Z2.5 to describe the soil response of deep alluvium deposits). Although, the ongoing efforts to elaborate such additional complementary parameters are promising (e.g., Thompson et al., 2011), V_{S30} still preserves its significance as an estimator to describe the overall effect of site on the ground-motion estimation.

The conventional method for implementing the site effects in ground-motion prediction models is to use the site amplification factors that are obtained by normalizing a chosen ground-motion intensity measure at a soil site with its counterpart measured at a nearby rock site (Borcherdt, 1970). The most important drawback of this approach is the lack of nearby rock sites while characterizing the site amplification for that specific event. One way of overcoming this drawback is to calibrate the ground motions at the site of interest by a geometrical spreading factor without modifying the particular site features to imitate their behavior at reference rock sites. This way the analyst can employ the conventional procedure by normalizing the amplitudes of calibrated ground motions with that of the reference rock site. Borcherdt (1994; 2002a; 2002b) and Dobry et al. (2000) utilized this

approach for the Loma Prieta and Northridge earthquakes and obtained the site factors that formed the basis of NEHRP site amplification factors (BSSC, 2003). Although, this procedure increases the number of usable recordings for site amplification studies, the likely regional dependency of geometrical spreading function may become critical for the reliable modification of the recordings that are collected from various regions of different crustal features.

Another efficient way of estimating the site effects on ground-motion amplitudes is to use stochastic methods for simulating different site conditions under different earthquake scenarios. Needless to say Boore and Joyner (1997) presented the groundbreaking and pioneer study in this field that proposes site amplification factors at different spectral frequencies using the quarter-wave length theory and stochastic simulations representing generic site classes. In more recent studies, Ni et al. (2000) and Walling et al. (2008) generate stochastic reference rock motions and convolve the soil motion associated with different features via site response analysis to modify the simulated rock motion. This way they derived site models for different soil conditions by modeling the site amplification between rock and soil motion through regressions on various functional forms. Following a similar concept Sokolov (1997; 2000) first simulated the reference rock motions at specific sites and then normalized the actual ground motions recorded at these sites with the generated reference rock simulations to derive his site amplification factors. Stochastic models may not fully address the complex source behavior and can be difficult to apply unless the concerned soil sites have been carefully investigated and are characterized by reliable geophysical and geotechnical tests. Nevertheless, they are still crucial to describe the functional form of the site model, provided they are based on the right

physics for the background nonlinear model, and the right order of magnitude for the corresponding soil nonlinear parameters. Moreover, such studies will certainly offer a better understanding of the physics behind the site response.

Alternative to the above approaches is the utilization of existing empirical ground-motion predictive models for describing the reference rock conditions to compute (or model) site amplification factors by normalizing the observed ground motions with the estimated reference rock motions. Studies conducted by Steidl (2000), Field (2000), Lee and Anderson (2000), Stewart et al. (2003) and Choi and Stewart (2005) consider this methodology either to observe the variation of site amplifications for different soil conditions or to derive site models for their use in GMPEs. Instead of employing the existing GMPEs to represent the reference rock motion, some studies derive specific predictive models to mimic different site conditions, including the reference rock, to compute the site factors through a similar normalization scheme as described above [e.g., Crouse and McGuire (1996); Rodriguez-Marek et al. (2001)]. Regardless of the implemented approach, all of these studies use V_{S30} as the main estimator parameter to describe the site influence on the ground-motion amplitude.

The main objective of this study is to propose an empirical site amplification function to be used for future pan-European GMPEs. The proposed model can capture the nonlinear soil effects as a function of V_{S30} for different input rock motion levels. The strong-motion database of this study is based on a subset of an extensive strong-motion databank that has been compiled in the framework of the Seismic Hazard Harmonization in Europe (SHARE) project. The selected subset includes recordings

from Europe and surrounding regions (Greek, Italian and Turkish strong-motion recordings) with measured shear-wave (S-wave) velocity information together with the strong-motion data collected from Taiwan, Japan and California with measured V_{S30} values for a broader coverage of soil behavior. The paper first describes the specific features of the used database and then extensively discusses the previous site models with special emphasis on the recent models developed in the **N**ext **G**eneration **A**ttenuation project (Power et al., 2008). The observations made from the NGA GMPEs on the soil behavior were used to derive the model presented here. The proposed site amplification function makes use of a reference rock model that is derived from a subset of the ground-motion database that results in a better description of the actual trends in the compiled database. This step is different in most of the similar studies because they either import the reference rock model from another research or use theoretical simulations to describe rock motion. The site amplifications computed by normalizing the observed data with the estimations obtained from the reference rock model are regressed by modifying the Walling et al. (2008) site function that is derived from the stochastic simulations. The empirically derived site model in this study confirms the results presented in Walling et al. (2008).

STRONG-MOTION DATABASE

The strong-motion database used in this study is extracted from a comprehensive ground-motion databank that has been compiled within the framework of the SHARE project (hereinafter SHARE SM databank). The SHARE SM databank consists of

shallow active crustal accelerograms gathered from the national and global databases that are listed in Table 1 with the relevant references. The metadata of the SHARE SM databank consists of event, station and strong-motion recording information as provided by these reference databases. The SHARE SM databank is composed of 2448 events and 14193 accelerograms recorded at 3708 stations. Only recordings corresponding to sites with measured S-wave velocities have been selected for the present study, leading to a subset of 5003 3-component accelerograms from 373 events recorded at 1503 sites. The moment magnitude range of the subset database is $4 \leq M_w \leq 7.9$. Small magnitude events ($M_w < 4.0$) were excluded in this study. The source-to-site distances of the selected recordings are $R_{JB} \leq 200$ km where R_{JB} is the closest distance to the surface projection of the rupture plane. The focal depth of the events was constrained to be less than 30 km and events that lack SoF information were discarded. Table 2 lists the magnitude, depth, SoF, V_{S30} and country based variation of the database in terms of number of events, records and stations. The details about the used database are described in the next paragraphs.

During the unification process of the SHARE SM databank, the duplicated event, station or waveform information in the reference databases was removed by the visual inspection of every entry. A hierarchical algorithm was developed while compiling the metadata: the information gathered from the local databases for the pertaining local events (e.g., T-NSMD for Turkish data, KIK-Net for Japanese data and ITACA for Italian data), is *a priori* judged to be the most relevant and reliable one. This is followed by the ESMD and ISESD databases for the European recordings as well as the NGA database for the accelerograms recorded in the rest

of the shallow active crustal regions (Yenier et al., 2010). Whenever the global databases (i.e., ESMD, ISESD and NGA) contain more complete event information for the earthquakes than the local databases, the priority for metadata information is given to the global databases.

The non-uniform style-of-faulting (SoF) classification in the reference databases was homogenized in the SHARE SM databank by applying the SoF definitions proposed in Boore and Atkinson (2007) that are based on the plunge angle (pl) of P- and T-axes as well as the rake angle (λ). The procedure prefers the use of plunge angle definitions for SoF classification and implements the rake angle information whenever the plunge angles cannot yield a definitive SoF. If, for a given event, the reference database lacks the moment-tensor solution (i.e., pl and λ angles cannot be computed), the SoF information provided by the reference database was accepted as is. In a similar fashion, if no information exists to compute pl and λ angles and if the unique information provided by the reference database is a SoF classification defined as normal-oblique or reverse-oblique, the former SoF classification is accepted as normal whereas the latter is designated as reverse in the SHARE SM databank.

Approximately 60% of the data originally did not have the calculated R_{JB} distance measure. For recordings that do not have R_{JB}, the procedure given in Kaklamonos et al. (2011) was applied that is primarily based on the double-couple fault-plane solutions. If the correct fault plane is provided by the reference database (approximately 40% of the data), this information was directly used to compute the extended-source distances. When the correct fault plane is unknown, R_{JB} is

computed for both planes. Figure 1 shows the R_{JB} ratios computed for both fault planes for the recordings that do not have a definite fault plane. These recordings constitute almost 35% of the data used in this study. The ratio scatters are plotted against the R_{JB} values computed from one of the planes. The mean trend and the 95% confidence intervals about the mean advocate that for most cases the extended-source distances computed from the 2 planes yield very similar values. The red circles on this figure are the ratios that fall outside the $\pm$ 10% band about the unity and they constitute 2% of the total data. Consequently, for cases that have fault-plane solutions but lacking the actual fault plane information, the average of the extended-source distances computed from both planes was considered. Although, this decision is arguable, it led to a significant increase in the number of data that have measured V_{S30} values. For small magnitude recordings (i.e., $M_w \leq 5.5$), in the absence of double-couple fault-plane solutions (25% of the data), the extended-source distance measures were computed by an iterative procedure following the methodology suggested by Scherbaum et al. (2004). This effort resulted in an additional 3036 recordings (thus, the total number of data sums up to 5003 records as stated in the 1st paragraph of this section) to the database used in this study.

The upper limit of the usable spectral period range of the accelerograms is determined from the fraction of high-pass filter cut-off values. The fractions proposed in Akkar and Bommer (2006) that depend on the recording type (i.e., analog vs. digital) and site class were used for this purpose. Whenever this procedure is inapplicable, due to the missing recording type information, the upper limit of the usable period range was taken as 80% of the high-pass filter cut-off period (Abrahamson and Silva, 1997). The methodology described in Akkar et al. (2011)

was used to determine the lower limit of the usable spectral period range of the accelerograms. Akkar et al. (2011) suggest discarding the spectral ordinates of the recordings for periods less than 0.05s when the filtered to mean removed spectral ordinate ratio falls out of the 0.9-1.1 range. This criterion is slightly relaxed in this study by extending the limits to ±15%.

Table 3 shows the types of in-situ measurement techniques applied for the computation of S-wave velocity profiles at the strong-motion sites that are included in the database. The table also gives information about the exploration depth for the in-situ measurements. The in-situ measurement techniques of approximately 20% of the stations are not reported (last row in Table 3) in the database. These stations are almost exclusively from the NGA database. Since NGA database is a product of long-term efforts (Power et al., 2008), the reported V_{S30} values of these stations were treated as reliable in this study. The remaining stations that lack in-situ measurement information are from the ESMD (Ambraseys et al., 2004a) and ISESD (Ambraseys et al., 2004b) databases that are also known as well-documented strong-motion data sources. The V_{S30} values of sites whose S-wave profiles do not extend to 30 m were computed by extending the last layer of the profile to 30 m.

Figure 2 shows the M_w vs. R_{JB} scatters by grouping the data in 6 major V_{S30} intervals. Figure 3 shows the distribution of PGA with respect to V_{S30} in the entire database. The plots on these figures indicate that the number of accelerograms decreases for V_{S30} values above 800 m/s and below 180 m/s (7% and 4% of the total data, respectively). The majority of the recordings have V_{S30} values in between 180 m/s and 550 m/s (71% of the total data). The scatters in Figure 2 also depict that the

distance-dependent distribution of accelerograms is fairly uniform for $M_w \leq 7.0$. This homogenous distribution loosens towards larger magnitudes ($M_w > 7.0$), which is a common feature in the current empirical strong-motion databases

CURRENT SITE AMPLIFICATION FUNCTIONS WITH EMPHASIS ON THE NGA MODELS

The adoption of site effects in GMPEs evolved progressively. In early GMPEs, the site effects were addressed by defining two broad site classifications (soil and rock). As a recent example, Sadigh et al. (1997) determined the site coefficients by employing separate regressions on rock and soil datasets. Other ground-motion models accounted for the site influence by considering more detailed soil categories that are based on the V_{S30} intervals of major seismic provisions. In such GMPEs (e.g., Akkar and Bommer, 2010), the same source and path models were used and the differences arising from site effects are attributed to different soil coefficients for each site category. Boore et al. (1997), [BJF97], proposed a more complicated site model that is a continuous function of V_{S30} [Eq. (1)]. In this model, the logarithm of the site amplification, (*ln (Amp)*) is proportional to the logarithm of V_{S30} normalized by a period-dependent reference velocity, V_{LIN} (T). The period-dependent coefficients $a(T)$ and $V_{LIN}(T)$ are computed from regression analysis.

$$ln(Amp) = a(T)\,ln(V_{S30} / V_{LIN}) \quad (1)$$

The site-model proposed by BJF97 as well as the others described in the previous paragraph do not include the nonlinear soil behavior. To the best of authors' knowledge the Abrahamson and Silva (1997), [AS97], site function is the first model

that considers the nonlinear soil amplification by classifying the sites as rock and soil. AS97 describes the nonlinear site amplification in soil sites as a function of the level of input rock motion (PGA_{rock}). AS97 site function is given in Eq. (2) where period dependent coefficients, *a(T)* and *b(T)* are determined from regression analysis and the period independent coefficient, *c* is constraint as 0.03g for the entire period range.

$$ln(Amp) = a(T) + b(T)\,ln(PGA_{rock} + c) \quad (2)$$

Choi and Stewart (2005), [CS05], in a way, combined Eqs. (1) and (2) to obtain a site model that represents both linear and nonlinear site amplification. To this end, they proposed linear and nonlinear site terms that are functions of period and V_{S30} [Eq. (3)]. This functional form modifies the PGA_{rock} dependent logarithmic expression to account for the overall nonlinear soil response.

$$ln(Amp) = a(T)\,ln(V_{S30}/V_{LIN}) + b(V_{S30},T)\,ln(PGA_{rock}/0.1) \quad (3)$$

The amplification factors in CS05 are computed by normalizing the observed acceleration spectrum ordinates with the corresponding estimations obtained from the reference rock model of AS97. The reference rock definition of AS97 corresponds to an average V_{S30} value of 550 m/s (Walling et al., 2008). The functional form of the CS05 model is developed in two stages. In the first stage, for a given period and each pre-defined V_{S30} bin, the natural logarithms of the amplification factors is expressed as a linear function of the natural logarithm of the estimated PGA_{rock}. Then the slope of the linear function that is obtained from the ordinary least-squares regression is used to quantify the soil nonlinearity. These discrete slopes are used to describe the functional form of the nonlinear term in Eq. (3) (i.e., $b(V_{S30},T)$). In the second stage, the variation of the soil amplification with respect to V_{S30} is determined by regressing on the data whose PGA_{rock} are near

0.1g. In other words, at this level of input rock motion the amplification is described by the functional form, $a(T)ln(V_{S30}/V_{LIN})$, that represents the linear site amplification. Finally, a unified model that combines the linear and nonlinear soil effects is proposed and the model coefficients, V_{LIN} and $a(T)$, are determined by random-effects regression.

Boore and Atkinson (2008), [BA08], one of the model developers in the NGA project (Power et al., 2008), adopted the CS05 site model with some modifications. The period-dependent V_{LIN} parameter in CS05 is a fixed reference V_{S30} value in BA08 that is called as V_{REF} (V_{REF} = 760 m/s). The overall contribution of soil nonlinearity in BA08 is formulated for 3 levels of input rock motion (i.e., $PGA_{rock} \leq 0.03g$; $0.03g < PGA_{rock} \leq 0.09g$; $PGA_{rock} > 0.09g$). Furthermore, Boore and Atkinson (2008) modified the $b(V_{S30},T)$ term with a piece-wise linear function (referred to as b_{nl} in their terminology). Figure 4.a shows the PGA site amplifications of CS05 and BA08 at different PGA_{rock} levels. Figure 4.b compares the behavior of $b(V_{S30},T)$ with b_{nl} for T = 0.0 s. As it is inferred from Figure 4.a the CS05 model results in a kink in site amplification in the vicinity of V_{S30} = 520 m/s due to the observed discontinuity in the $b(V_{S30},T)$ term at this V_{S30} value. The BA08 model removes this behavior by introducing a smooth transition in b_{nl} between 300 m/s $\leq V_{S30} \leq$ 760 m/s (Figure 4.b). However, this smooth transition imposes lower nonlinear soil behavior with respect to CS05 for 300 m/s $\leq V_{S30} \leq$ 520 m/s. On the contrary, the linear trend in b_{nl} between 180 m/s $< V_{S30} <$ 300 m/s yields slightly higher soil nonlinearity with respect to CS05. Figure 4.a also shows that BA08 results in higher amplification levels with respect to those of CS05 when V_{S30} attains larger values (i.e., V_{S30} > 300 m/s). This behavior can be attributed to the modifications to the V_{LIN} parameter because linear

site behavior generally governs for V_{S30} > 300 m/s as will be discussed in the following paragraphs. This observation suggests that the BA08 model presumably estimates larger site amplifications for linear soil behavior. In fact the use of period-independent V_{REF} in BA08 seems to shift the site amplifications towards higher values for the entire V_{S30} band at all rock PGA levels except for those of low V_{S30} sites subjected to low ground-motion amplitudes (mimicked by $PGA_{rock} \leq 0.03g$ in Figure 4.a). For very low ground-motion amplitudes the BA08 model prevents the increase in soil nonlinearity at softer sites by imposing a constant nonlinear amplification at the lowest range of input rock motion (i.e., $PGA_{Rock} \leq 0.03g$). This fact is not accounted for CS05. The lower bound of V_{S30} for CS05 and BA08 is 180 m/s however the plots on Figure 4 extend V_{S30} towards much smaller values to show the behavior of these models if they are used for addressing the low-velocity site amplification.

The site model proposed by Chiou and Youngs (2008), [CY08], is also developed within the framework of NGA project and it is similar to CS05. CY08 derived their functional form by interpreting the studies of BJF97 and AS97. The reference velocity (V_{REF}) that is considered as 760 m/s in BA08 is 1130 m/s in CY08 by assuming that no major soil nonlinearity can take place beyond this velocity level. The site amplification is set to unity for V_{S30} values greater than V_{REF}. Contrary to BA08 that uses the site coefficients of CS05, the proponents of this model determined the site coefficients by regressing on their own database that led to the better representation of the data trend. The nonlinear site response term has a simpler format with respect to BA08 and it is expressed by a reference rock spectral acceleration (instead of the reference rock PGA) at the period of interest.

In the context of the NGA project, Walling et al. (2008), [WAS08], also proposed a site model. Walling et al. (2008) generated stochastic simulations to obtain the rock motions at V_{S30} = 1100 m/s and performed site response analysis to obtain the soil motions at certain V_{S30} values. In site response analysis, four specific modulus reduction and damping curves were used to mimic the site conditions in (Imperial Valley, Bay Mud, Peninsular range and EPRI models). The first and second degradation curves were used when V_{S30} < 270 m/s. The third and fourth curves represent the cases when V_{S30} ≥ 270 m/s. The site amplification was calculated by dividing the convoluted soil motions by the simulated reference rock motions. These amplification factors were then utilized to derive the site model as two piece-wise functional forms with the following major assumptions: the response of soil becomes linear as PGA_{rock} goes to zero and after a certain value of V_{S30} that is defined by the V_{LIN} parameter (when $V_{S30} \geq V_{LIN}$ the soil response is assumed to be linear). Equation 4 shows the model proposed by WAS08. It should be noted that WAS08 selects PGA_{rock} as the main controlling parameter in soil nonlinearity for all spectral periods. The coefficients *a(T)*, *b(T)*, *c* and *n* are the regression coefficients. The parameter *d* implicitly relates the linear transition between $V_{LIN}(T)$ and the reference rock site shear-wave velocity that is taken as 1100 m/s.

$$\ln(Amp) = \begin{cases} a(T)\ln(V_{S30}/V_{LIN}) - b(T)\ln(PGA_{rock}+c) \\ +\, b(T)\ln(PGA_{rock}+c(V_{S30}/V_{LIN})^{n}) + d & \text{for } V_{S30} < V_{LIN} \\ (a(T)+b(T)n)\ln(V_{S30}/V_{LIN}) + d & \text{for } V_{S30} \geq V_{LIN} \end{cases} \quad (4)$$

The WAS08 nonlinear site model was implemented in the Campbell and Bozorgnia (2008) and Abrahamson and Silva (2008) [CB08 and AS08, respectively] GMPEs. In their site models, AS08 and CB08 used the nonlinear soil coefficients derived from the Peninsular range shear modulus and damping degradation curves. The major difference between the AS08 and CB08 models stems from the linear site term

because they used different subsets of the NGA database. The use of different functional forms for describing the source and path effects as well as different regression techniques can also play a role in these differences. As these two models have the same origin for site response, the results obtained from AS08 are presented in the content of this study. The site amplification factors of AS08 model are lower than unity at V_{S30} = 1100 m/s. The reason behind this behavior is that AS08 does not consider the *d* term proposed in WAS08. As a matter of fact the *d* term is compensated by other regression coefficients (e.g., source and path coefficients) in the ground-motion prediction model of AS08. Since one of the aims of this study is the evaluation of different site models, this parameter is included in AS08 in order to observe an amplification ratio of unity at V_{S30} = 1100 m/s. Besides, AS08 adds another period dependent V_{S30} parameter, V_{CON}, above which the site term becomes constant. Consequently, for $V_{S30} < V_{LIN}$ the amplification is a function of PGA_{rock} and V_{S30}. For V_{S30} values between V_{LIN} and V_{CON}, the amplification depends only on V_{S30} (i.e., only linear amplification). For $V_{S30} > V_{CON}$ a constant amplification is imposed by this model whatever the PGA_{rock} and V_{S30} values.

Figures 5 to 7 show the site amplification factors obtained from BA08, CY08, and AS08, respectively. In these figures, the left column illustrates the variation of amplification factors for several input rock motion levels as a function of V_{S30}. The middle and right columns show the variation of site amplifications for a wide range of V_{S30} values as a function of input rock motion level. The panels in the middle column consider low V_{S30} values ranging between 200 m/s ≤ V_{S30} ≤ 280 m/s whereas the V_{S30} ranges in the right column vary from 300 m/s ≤ V_{S30} ≤ 1100 m/s. Each row in Figures 5-7 displays the variation of site amplification for a selected period value. For

BA08 model (Figure 5), the soil nonlinearity is dominant for sites with V_{S30} < 300 m/s. The contribution of soil nonlinearity to site amplification decreases with increasing period when V_{S30} values are greater than 300 m/s. The influence of soil nonlinearity seems to vanish completely beyond T = 1.0 s and no nonlinear site effect is considered for V_{S30} > 760m/s. For sites that are located on very soft soil (i.e., V_{S30} < 180 m/s) the amplification trend changes and starts to increase with increasing PGA_{rock}, which is due to the use of constant nonlinear coefficient in this range. The middle column panels in Figure 5 indicate that the amplification becomes independent of V_{S30} at a certain value of PGA_{rock}. This input rock motion level is called as hinging PGA in this article and it is a function of period. For PGA_{rock} values that are lower than this hinging PGA, the linear site term dominates and softer sites show higher amplification. Beyond the hinging PGA the contribution of nonlinear term increases for soft sites with low V_{S30} values. As the stiffness of the site increases, the hinging PGA shifts to a larger value. This observation indicates that for stiffer sites BA08 model does not expect nonlinear soil behavior except for very strong ground motions associated with high PGA_{rock}. The hinging PGA shifts towards larger values with increasing period for V_{S30} < 300 m/s. The same trend is also observed for 300 m/s < V_{S30} < 760 m/s at higher levels of input rock motion but in this case the amplitude of hinging PGA decreases with increasing period and vanishes after T > 1.0 s. This observation suggests that BA08 model barely expects nonlinear soil behavior (i.e., PGA_{rock} values larger than hinging PGA) for stiff sites.

Figure 6 illustrates the site amplifications computed from CY08. The CY08 site model shows neither amplification nor de-amplification for V_{S30} > V_{REF} (=1130 m/s). The overall behavior of CY08 indicates that this model expects significant soil

nonlinearity for V_{S30} < 360 m/s. For softer sites (i.e., V_{S30} < 300 m/s) there is also a hinging PGA in this model whose value increases with increasing period. For stiffer sites hinging PGA is not observed in CY08. The contribution of soil nonlinearity in CY08 decreases with increasing period. Figure 7 shows the variation of site amplifications for AS08. The V_{LIN} and V_{CON} parameters in AS08 decreases with increasing period, which indicates that this model does not expect nonlinear soil behavior at long periods. As in the case of other models discussed in the above text, the contribution of nonlinearity increases with decreasing period and increasing PGA_{rock} in AS08. The site amplification behavior in the middle column panels of Figure 7 suggests that the AS08 site amplification becomes independent of V_{S30} for $PGA_{rock} \approx 0.2g$ and this trend can also be considered as the hinging PGA behavior.

PROPOSED SITE MODEL AND ITS EVALUATION

As summarized in the previous section Boore et al. (1997) and Abrahamson and Silva (1997) introduced the base models for the linear and nonlinear soil behavior. These models formed the basis of site functions in the Choi and Stewart (2005) and Walling et al. (2008) studies. BA08 and CY08 modified CS05 such that the effects of V_{S30} and the level of input rock motion are considered separately in the nonlinear part of their models. On the other hand, Walling et al. (2008) proposed a nonlinear soil model in which these two parameters are formulated in one expression. All of these models generally show similar trends in the site amplification factors and the differences in these factors primarily stem from the data used in each study. The model presented here favors the functional form proposed by WAS08 because it is

relatively simpler with respect to other models. The WAS08 model is calibrated by considering the limitations in the database, the interpretations made on the observed amplification trends that are discussed in the previous section and the observed residual trends in the regression analyses. The following paragraphs describe the steps and the methodology implemented to finalize the functional form of the site model.

Instead of using a period dependent reference velocity (V_{LIN}) as proposed by WAS08, a period independent reference velocity (V_{REF}) is preferred in the presented model. This assumption also eliminates the need for the *d* term in WAS08. Besides, the PGA_{rock} parameter is changed to Y_{REF} (in g; gravitational acceleration) that is the level of input rock motion at the reference value of V_{S30} at the period of interest. This parameter will be discussed later in the text.

A set of preliminary analyses was made before bringing the proposed model to its final format. Firstly, the nonlinear terms were set to 0 (i.e., $b(T) = 0$) in order to see the capability of the used database in addressing the nonlinear site effects. This first-stage analysis showed that the increase in the level of input rock motion results in reduced site amplification factors indicating the existence of nonlinear behavior in soil sites. This observation also indicated the adequacy of the database to capture the nonlinear soil behavior. The residuals of this preliminary study also revealed relatively lower site amplification estimations at high V_{S30} values. Thus, the site amplification was held fixed for higher V_{S30} values after this particular study. This behavior is also observed in AS08. Although, the number of data is inadequate to determine the limiting shear-wave velocity (V_{CON}) after which the amplification is

constant, it is decided to constrain it as 1000 m/s. In the second-stage analysis, the soil nonlinearity was taken into account. The input rock motion (Y_{REF}) was taken either as the estimations of the reference rock motion at T = 0.0 s or the spectral ordinates at the period of interest (i.e., $Y_{REF} = PGA_{REF}$ or $Y_{REF} = PSA_{REF}$). The site models computed from these two alternative cases showed that both models follow the general trends of the observed data and there is no specific difference between these models. Since the site model that is based on PGA_{REF} is simpler than the other alternative, $Y_{REF} = PGA_{REF}$ was used as the reference input rock motion. The final functional form of the proposed model is given in Eq. (5).

$$ln(Amp) = \begin{cases} a(T)\,ln(V_{S30}/V_{REF}) \\ +b(T)\,ln\left[\dfrac{PGA_{REF}+c(V_{S30}/V_{REF})^n}{(PGA_{REF}+c)(V_{S30}/V_{REF})^n}\right] & \text{for } V_{S30} < V_{REF} \\ a(T)\,ln(V_{S30}/V_{REF}) & \text{for } V_{REF} \le V_{S30} < V_{CON} \\ a(T)\,ln(V_{CON}/V_{REF}) & \text{for } V_{S30} \ge V_{CON} \end{cases} \quad (5)$$

where *a(T), b(T), c* and *n* are regression coefficients. The parameter, $V_{REF,}$ is the period independent reference velocity (V_{REF}). PGA_{REF} (in g; gravitational acceleration) is the level of input rock motion at the reference value of V_{S30} and it is estimated from the reference rock ground-motion model from the dataset used in this study. The coefficient *c* provides the transition between higher and lower ground-motion amplitudes. The parameter *n* mainly captures the soil nonlinearity at low V_{S30} sites.

The reference velocity was initially chosen as V_{S30} = 800 m/s (A/B class boundary in EC8; CEN, 2003) for the site model. However, the database has a limited number of recordings in the vicinity of the specified V_{S30} value both for smaller distances and larger magnitudes as presented in Figure 2. Thus, the reference velocity was taken

as 600 m/s [soft-rock condition according to Walling et al. (2008)]. The recordings from sites whose V_{S30} values are between 550 and 650 m/s were selected as a subset of the entire database to derive the ground-motion model for estimating the reference rock motion (see Figure 2, middle row, left column). The site amplifications were determined by normalizing the observed spectral ordinates with the corresponding median estimations of the reference rock ground-motion model. This model also defines PGA_{REF}. A functional form similar to the one proposed by Akkar and Bommer (2010) was used for the derivation of reference rock ground-motion model (Eq. 6).

$$\ln Y = a_1 + a_2(M-5) + a_3(M-5)^2 + [a_4 + a_5(M-5)]\ln\sqrt{R^2 + a_6{}^2} + a_7 F_N + a_8 F_R \qquad (6)$$

Equation 6 includes quadratic magnitude scaling and magnitude dependent distance decay term with fictitious depth. As the source-to-site distance, R_{JB} was preferred and the SoF effect is represented by the dummy variables in the model. The reference rock model coefficients were obtained from the random-effects regression analysis (Abrahamson and Youngs, 1992). Figure 8 shows the between- and within-event residual distributions for T = 0.0 s and spectral ordinates at 0.2 s and 1.0 s. No obvious trends are observed in the between-and within-event residuals that are plotted as functions of M_w and R_{JB}, respectively. Figure 9 compares the derived reference rock ground-motion model with the 3 NGA GMPEs for V_{S30} = 600 m/s. The comparisons are done for a fictitious strike-slip fault with a dip angle of 90º and the site is placed on the footwall side. The differences in the distance measures among the compared GMPEs were taken into account based on the simple scenario described here. Default values proposed by the model developers were used for some particular estimator parameters (e.g., Z1.0) that are employed in the NGA GMPEs. Although the database used for the reference rock model is limited due to

sparsely distributed high-V_{S30} data, the reference rock estimations between the NGA GMPEs and the ground-motion model derived in this study are fairly comparable. The rock ground-motion model derived in this study yields slightly lower estimations with respect to other GMPEs for small (M_w = 5) and intermediate (M_w = 6.5) magnitude events as the period shifts towards longer period range (T = 1.0 s). On the contrary, for strong events the estimations are higher than the NGA models but this trend gradually diminishes at longer periods.

The site amplification factors that are calculated using the observed data and the estimated reference rock motions at V_{S30} = 600 m/s were then used to obtain the site model coefficients by applying the random-effects regression analysis. The coefficients *c* and *n* were only computed at T = 0.0 s and held fixed for the entire period range because PGA_{REF} describes the input rock motion level in the proposed model. The site model is derived for 63 spectral periods between 0.0 s ≤ T ≤ 4.0 s and for PGV. The regression coefficients for the selected periods are given in Table 4. The corresponding within- and between-event standard deviations (σ and τ, respectively) at these periods are also listed in the same table. As it can be inferred from Table 4, the *b(T)* coefficient that controls the nonlinear soil behavior increases with increasing period up to T = 0.3 s. This coefficient tends to decay towards longer periods. A similar behavior is also observed in WAS08, which indicates that the nonlinear site behavior derived from the empirical data of this study is consistent with the stochastic simulations of the WAS08 model. The top row in Figure 10 shows the between-event residual scatters of the proposed model as a function magnitude. The middle and bottom rows in the same figure display the within-event residual distributions with respect to R_{JB} and V_{S30}, respectively. Each column in Figure 10

shows the variation of residuals for periods of T = 0.0 s, T = 0.2 s and T = 1.0 s. The residual trends in these particular spectral periods would give an overall idea about the success of the proposed model. The residual plots in Figure 10 advocate that the site amplifications estimated by the model are unbiased as the variations in residuals are random in terms of the selected seismological and geotechnical parameters.

Figure 11 compares the proposed model (black line) and the variation of the data for different PGA_{REF} intervals. The comparisons are done for T = 0.0 s (first row) and spectral ordinates at 0.2 s and 1.0 s (middle and bottom row, respectively). For the first two periods, the nonlinear soil behavior is dominant. The nonlinearity in soil behavior diminishes significantly for periods beyond T = 1.0 s, and almost vanishes for T > 2.0s. The figure also includes two other site models for comparison: AS08 (red line) and BA08 (green line). The site models of BA08 and AS08 were modified to obtain amplification factors consistent with 600 m/s (i.e., V_{REF} in this study). The modifications to BA08 and AS08 were done carefully without losing their nonlinear soil features. The immediate observation from Figure 11 is that the estimated site amplifications of the proposed model are comparable with AS08 and BA08. Moreover all models seem to follow the data trend closely for $V_{S30} \leq 1000$ m/s. In general, for low V_{S30} values ($V_{S30} \leq 300$ m/s), the site amplifications of the proposed model are slightly lower than those of AS08 and BA08. This observation suggests that the derived model indicates a slightly higher nonlinearity as sites get softer. The proposed model is derived using the data points given in these figures, so the relatively close match between the data and the estimations of the model should be expected. The other reason of discrepancy between the data and the 2 NGA models could be their lower-bound V_{S30} values. The lowest V_{S30} value for both models is

approximately 180 m/s that is slightly higher than the minimum V_{S30} value given in these plots. For increasing V_{S30} values (V_{S30} > 300 m/s), when the soil behavior is presumably linear, all models yield similar amplification factors. When V_{S30} attains relatively large values ($V_{S30} \geq 1000$ m/s) the site model presented in this study as well as AS08 cap the site amplification to a constant value (to prevent very small amplification factors).

As a final plot, Figure 12 compares the period-dependent standard deviation of the proposed model with those given CS05. The figure does not include the NGA models as they do not specifically compute the standard deviations for their site amplification functions. This is because their site models are presented as part of their GMPEs. (Within the NGA models investigated here, AS08 assumes that the standard deviation of their site model is 0.3. Both AS08 and CY08 models consider a decrease in the total standard deviation as the nonlinear soil behavior dominates). The comparative plots in Figure 12 indicate that the standard deviation of the proposed model is higher than that of CS05

SUMMARY AND CONCLUSION

This study presents an empirical site amplification model that can be used in the next pan-European GMPEs. The functional form is capable of addressing the linear and nonlinear soil behavior and it is based on a well-studied extensive dataset with the most recent updates of the Greek, Italian and Turkish site information, considering only sites with measured S-wave velocity. A particular ground-motion model is also

derived to estimate the level of input rock motions that are used in the calculation of the site amplification factors. The reference rock ground-motion model is capable of representing the trends in the used dataset and gives comparable estimations with the NGA GMPEs. In fact, the derived model directly reflects the overall linear and nonlinear soil features of the observed data; neither the previously derived site expressions nor additional synthetic data were imported to augment the model behavior. The presented model is based on WAS08 after a detailed investigation of the earlier site amplification models. The simplicity of WAS08 site model is the major reason behind its choice. The proposed model is entirely based on an empirical dataset and the results are consistent with those of the WAS08, which uses synthetic data. This fact can advocate the robustness and the reliability of the model in addressing the genuine soil behavior.

The chosen dataset is capable of addressing the nonlinear soil behavior as the initial runs that disregard nonlinearity in the proposed model resulted in decreasing site amplifications with the increased levels of input rock motion. The model assigns constant site amplification for sites with V_{S30} greater than 1000 m/s and describes the input rock motion in terms of PGA (PGA_{REF}) as no significant difference was observed in the estimated site amplifications when input rock motion is defined in terms of the spectral ordinates at each specific period. The use of PGA_{REF} as the input rock motion also simplifies the model. The comparisons between the proposed model and those given in the literature yield consistent results with some variations in very soft site amplifications when the soil nonlinearity becomes prominent at high intensities. The proposed model estimates a slightly higher nonlinearity in the soil behavior in such cases.

REFERENCES

Abrahamson, N.A. and Silva, W. (2008). Summary of the Abrahamson and Silva NGA ground motion relations, *Earthquake Spectra*, **24**: 67-98.

Abrahamson, N.A. and Silva, W.J. (1997). Empirical response spectral attenuation relations for shallow crustal earthquakes, *Seismological Research Letters*, **68**: 94-127.

Abrahamson, N.A. and Youngs, R.R. (1992). A stable algorithm for regression analyses using the random effects model, *Bulletin of the Seismological Society of America*, **82**: 505–510.

Akkar, S., and Bommer, J.J. (2006). Influence of long-period filter cut-off on elastic spectral displacements, *Earthquake Engineering and Structural Dynamics*, **35**: 1145-1165.

Akkar, S., Çağnan, Z., Yenier, E., Erdogan, E., Sandıkkaya, M.A., and Gülkan, P. (2010). The recently compiled Turkish strong-motion database: preliminary investigation for seismological parameters, *Journal of Seismology*, **14**: 457-479.

Akkar, S., Kale, Ö., Yenier, E., and Bommer, J.J. (2011). The high-frequency limit of usable response spectral ordinates from filtered analogue and digital strong-motion accelerograms, Earthquake Engineering and Structural Dynamics, **40**: 1387 – 1401.

Ambraseys N.N. , Douglas J., Sigbjörnsson R., Berge-Thierry C., Suhadolc P., Costa G., Smit P., (2004a). Dissemination of European Strong Motion Data Vol:2 Using Strong Motion Datascape Navigator. CD-ROM collection, Feb. Engineering and Physical Sciences Research Council, United Kingdom.

Ambraseys N.N., Smit, P., Douglas J., Margaris B, Sigbjörnsson R., Olafsson, S., Suhadolc, P., and Costa, G. (2004b). Internet site for European strong-motion data, *Bollettino di Geofisica Teorica ed Applicata*, **45**: 113-129.

Boore, D.M. and Atkinson, G.M. (2007). Boore-Atkinson NGA Ground Motion Relations for the Geometric Mean Horizontal Component of Peak and Spectral Ground Motion Parameters, PEER 2007/01, Pacific Earthquake Engineering Research Center, University of California, Berkeley, California.

Boore, D.M. and Atkinson, G.M. (2008). Ground-Motion Prediction Equations for the Average Horizontal Component of PGA, PGV, and 5%-Damped PSA at Spectral Periods between 0.01s and 10.0s, *Earthquake Spectra*, **24**: 99-138.

Boore, D.M. and Joyner, W.B. (1997). Site Amplifications for Generic Rock Sites, *Bulletin of the Seismological Society of America*, **87**: 327 - 341.

Boore, D.M., Joyner, W.B. and Fumal, T.E. (1997). Equations for estimating horizontal response spectra and peak acceleration from western North American earthquakes: a summary of recent work. *Seismological Research Letters*, **68**: 128-153.

Borcherdt, R.D. (1970). Effects of local geology on ground motion near San Francisco Bay, *Bulletin of the Seismological Society of America*, **60**: 29-61.

Borcherdt, R.D. (1994). Estimates of Site Dependent Response spectra for Design (Methodology and Justification), *Earthquake Spectra*, **10**: 617-653.

Borcherdt, R.D. (2002a). Empirical evidence for acceleration-dependent amplification factors, *Bulletin of the Seismological Society of America*, **92**: 761-782.

Borcherdt, R.D. (2002b), Empirical evidence for site coefficients in building-code provisions, *Earthquake Spectra*, **18**: 189-218.

BSSC, Building Seismic Safety Council (2003). NEHRP Recommended Provisions for Seismic Regulations for New Buildings and Other Structures, FEMA-450, 2003 revision, Federal Emergency Management Agency, Washington D.C.

Campbell, K.W. and Bozorgnia, Y. (2008). NGA ground motion model for the geometric mean horizontal component of PGA, PGV, PGD and 5% damped linear elastic response spectra for periods ranging from 0.01 to 10 s, *Earthquake Spectra*, **24**: 139-171.

Cauzzi, C. and Faccioli, E. (2008). Broadband (0.05 to 20 s) prediction of displacement response spectra based on worldwide digital records, *Journal of Seismology*, **12**: 453-475.

CEN, European Committee for Standardization, (2003). "Eurocode 8: Design of structures for earthquake resistance - Part 1: General rules, seismic actions and rules for buildings", European Committee for Standardization, Brussels.

Chiou, B., Darragh, R., Gregor, N., and Silva, W. (2008) NGA Project Strong-Motion Database, *Earthquake Spectra*, **24**: 23-44.

Chiou, B.S.-J. and Youngs, R. (2008). An NGA model for the average horizontal component of peak ground motion and response spectra, *Earthquake Spectra*, **24**: 173-215.

Choi, Y. and Stewart, J.P. (2005). Nonlinear site amplification as function of 30m shear wave velocity, *Earthquake Spectra*, **21**: 1-30.

Crouse, C.B. and McGuire, J.W. (1996). Site response studies for purpose of revising NEHRP seismic provisions, *Earthquake Spectra*, **12**: 407-439.

Dobry, R., Borcherdt, R.D., Crouse, C.B., Idriss, I.M., Joyner, W.B., Martin, G.R., Power, M.S., Rinne, E.E., and Seed, R.B. (2000). New site coefficients and site classification system used in recent building seismic code provisions, *Earthquake Spectra*, **16**: 41-67.

Field, E.H. (2000). A Modified Ground-Motion Attenuation Relationship for Southern California that Accounts for Detailed Site Classification and a Basin-Depth Effect, *Bulletin of the Seismological Society of America*, **90**: S209-S221.

Kaklamanos, J., Baise, L.G., and Boore, D.M. (2011). Estimating unknown input parameters when implementing the NGA ground-motion prediction equations in engineering practice. *Earthquake Spectra*, (in press).

Lee, Y., and Anderson, J.G. (2000). Potential for Improving Ground-Motion Relations in Southern California by Incorporating Various Site Parameters, *Bulletin of the Seismological Society of America*, **90**: S170-S186.

Ni, S-D., Anderson, J.G., Zeng, Y., and Siddharthan, R.V. (2000). Expected Signature of Nonlinearity on Regression for StrongGround-Motion Parameters, *Bulletin of the Seismological Society of America,* **90:** S53-S64.

Pousse, G., Thierry, C.B and Bard, P.-Y. (2005). Eurocode 8 Design response spectra evaluation using the K-NET Japanese database, *Journal of Earthquake Engineering*, **9**: 547-574.

Power, M., Chiou, B., Abrahamson, N., Bozorgnia, Y., Shantz, T., and Roblee, C. (2008). An Overview of the NGA Project, *Earthquake Spectra*, **24**: 3-21.

Rodriguez-Marek, A., Bray, J. D., and Abrahamson N. A. (2001). An empirical geotechnical seismic site response procedure, *Earthquake Spectra*, **17**: 65-87.

Sadigh, K., Chang, C.Y., Egan, J. A., Makdisi, F., and Youngs, R.R. (1997). Attenuation relationships for shallow crustal earthquakes based on California strong motion data, *Seismological Research Letters*, **68**: 180-189.

Sandıkkaya, M.A., Yılmaz, M.T., Bakır, B.B., and Yılmaz, Ö. (2010). Site classification of Turkish national strong-motion stations, *Journal of Seismology*, **14**: 543-563.

Scherbaum, F., Schemedes, J., and Cotton, F. (2004). On the Conversion of Source-to-Site Distance Measures for Extended Earthquake Source Models, *Bulletin of the Seismological Society of America*, **94**: 1053 - 1069.

Sokolov, V.Y. (1997). Empirical models for estimating Fourier-amplitude spectra of ground acceleration in the northern Caucasus (Racha seismogenic zone), *Bulletin of the Seismological Society of America*, **87**: 1401-1412.

Sokolov, V.Y. (2000). Hazard-Consistent Ground Motions: Generation on the Basis of Uniform Hazard Fourier Spectra, *Bulletin of the Seismological Society of America*, **90**: 1010 - 1027.

Steidl, J.H. (2000). Site Response in Southern California for Probabilistic Seismic Hazard Analysis, *Bulletin of the Seismological Society of America*, **90**: S149-S169.

Stewart, J.P., Liu, A.H., and Choi, Y. (2003). Amplification Factors for Spectral Acceleration in Tectonically Active Regions, *Bulletin of the Seismological Society of America*, **93**: 332-352.

Thompson, E.M., Baise, L.G., Kayen, R.E., Morgan, E.C., and Kaklamanos, J. (2011). Multiscale Site Response Mapping: A case study of Parkfield, California, *Bulletin of the Seismological Society of America*, **101**: 1081 - 1100.

Walling, M., Silva, W., and Abrahamson, A. (2008). Nonlinear Site Amplification Factors for Constraining the NGA Models, *Earthquake Spectra*, **24**: 243-255.

Working Group ITACA (2010) - Data Base of the Italian strong motion records: http://itaca.mi.ingv.it

Yenier, E., Sandıkkaya, M.A., and Akkar, S. (2010). Report on the fundamental features of the extended strong-motion databank prepared for the SHARE Project. Workshop for WP4, Ankara, Turkey.

TABLES

Table 1. Strong-motions datasets gathered in the SHARE SM databank.

Dataset	Number of Events	Number of Recordings	Reference
European **S**trong **M**otion **D**atabase (ESMD)	45	214	Ambraseys et al. (2004a)
Internet **S**ite for **E**uropean **S**trong-motion **D**ata (ISESD)	675	2046	Ambraseys et al. (2004b)
ITalian **AC**celerometric **A**rchive database (ITACA)	199	1165	Working Group ITACA (2010)
K-Net Database	27	987	National Research Institute for Earth Science and Disaster Prevention*
KiK-Net database	596	4704	National Research Institute for Earth Science and Disaster Prevention**
Next **G**eneration **A**ttenuation database (NGA)	152	3403	Chiou et al. (2008)
Turkish **N**ational **S**trong-**M**otion **D**atabase (T-NSMD)	754	1674	Akkar et al., (2010); Sandıkkaya et al. (2010)

*The data used within this study is selected by Cauzzi and Faccioli. (2008)
**The data used within this study is selected by Pousse et al. (2005)

Table 2. Some important statistics about the used database in this study

Magnitude Range	**N_E***	**N_R***
$M_w < 5.0$	153	1393
$5.0 \le M_w < 6.0$	163	1815
$6.0 \le M_w < 7.0$	43	1470
$7.0 \le M_w < 8.0$	14	325
Depth range (km)	**N_E***	**N_R***
$0 \le D \le 5$	106	1624
$5 < D \le 10$	108	1486
$10 < D \le 15$	85	1200
$15 < D \le 20$	43	561
$20 < D \le 25$	15	54
$25 < D \le 30$	16	78
Style-of-Faulting	**N_E***	**N_R***
Normal	101	603
Reverse	119	2660
Strike-Slip	153	1740
Country	**N_E***	**N_R***
Greece	33	117
Italy	55	312
Japan	142	2954
Taiwan	6	684
Turkey	88	467
USA	42	431
Others	7	38
V_{S30} range (m/s)	**N_S***	**N_R***
$V_{S30} \le 180$	79	179
$180 < V_{S30} \le 360$	566	1705
$360 < V_{S30} < 550$	537	1829
$550 \le V_{S30} \le 650$	108	484
$650 < V_{S30} \le 800$	108	471
$V_{S30} > 800$	105	335

* N_E: number of events, N_R: number of recordings, N_S: number of stations

Table 3. Types of measurements that applied to compute the S-wave velocity profiles of the sites used in this study. Exploration depth information is also included in the table.

In-situ measurement	Exploration Depth <30 m	Exploration Depth >30 m	Unknown
Cross-hole	1	24	-
Down-hole	426	551	-
MASW *	-	111	-
SASW **	3	4	-
SLT ***	5	17	-
Others	3	10	-
Unknown	2	260	86

* Multi-channel analysis of surface waves
** Spectral analysis of surface waves analysis
*** Suspension logging test

Table 4. Regression coefficients and corresponding standard deviations for the site amplification model. The within- and between-event sigmas are denoted as σ and τ, respectively, and σ_T is the total standard deviation.

Period	a	b			τ
PGA	-0.38649	-0.32699	0.6286	0.4701	0.7849
PGV	-0.77882	-0.37265	0.5691	0.4172	0.7056
0.01	-0.38340	-0.32292	0.6291	0.4705	0.7856
0.02	-0.36075	-0.29823	0.6294	0.4772	0.7899
0.03	-0.29722	-0.24354	0.6343	0.4810	0.7961
0.04	-0.21963	-0.20516	0.6423	0.4924	0.8093
0.05	-0.15316	-0.17333	0.6505	0.5091	0.8260
0.075	-0.08585	-0.10904	0.6892	0.5530	0.8836
0.1	-0.22862	-0.34275	0.7090	0.5730	0.9116
0.11	-0.27350	-0.40804	0.7059	0.5840	0.9162
0.12	-0.31212	-0.44418	0.7055	0.5783	0.9122
0.13	-0.36631	-0.50272	0.7072	0.5715	0.9093
0.14	-0.40717	-0.52611	0.7057	0.5648	0.9039
0.15	-0.44877	-0.53099	0.7041	0.5539	0.8959
0.16	-0.49206	-0.55068	0.7019	0.5493	0.8913
0.17	-0.53318	-0.57522	0.6998	0.5350	0.8809
0.18	-0.57055	-0.59085	0.6970	0.5199	0.8695
0.19	-0.60883	-0.61194	0.6957	0.5101	0.8627
0.2	-0.64130	-0.62912	0.6942	0.5000	0.8555
0.22	-0.68355	-0.63690	0.6897	0.4953	0.8491
0.24	-0.72928	-0.66131	0.6833	0.4862	0.8386
0.26	-0.77708	-0.68514	0.6803	0.4780	0.8314
0.28	-0.81352	-0.66760	0.6741	0.4751	0.8247
0.3	-0.83769	-0.64686	0.6677	0.4751	0.8195
0.32	-0.85822	-0.63604	0.6632	0.4719	0.8140
0.34	-0.88111	-0.62699	0.6616	0.4693	0.8111
0.36	-0.89261	-0.61568	0.6606	0.4729	0.8124
0.38	-0.90579	-0.61464	0.6602	0.4755	0.8136
0.4	-0.91908	-0.60700	0.6584	0.4770	0.8130
0.42	-0.93951	-0.61163	0.6539	0.4780	0.8100
0.44	-0.95691	-0.60702	0.6493	0.4802	0.8076
0.46	-0.96511	-0.58875	0.6458	0.4789	0.8040
0.48	-0.97933	-0.58461	0.6430	0.4769	0.8006
0.5	-0.99469	-0.58066	0.6403	0.4789	0.7996
0.55	-1.02144	-0.58252	0.6359	0.4796	0.7965
0.6	-1.04326	-0.56136	0.6320	0.4819	0.7948
0.65	-1.05682	-0.50881	0.6313	0.4813	0.7938
0.7	-1.06742	-0.46281	0.6297	0.4800	0.7918

Table 4. (Cont'd)=

Period	a	b			$_T$
0.75	-1.07456	-0.46361	0.6270	0.4702	0.7837
0.8	-1.07705	-0.46547	0.6273	0.4679	0.7826
0.85	-1.08557	-0.46624	0.6293	0.4680	0.7842
0.9	-1.09541	-0.47011	0.6315	0.4670	0.7854
0.95	-1.09476	-0.46318	0.6346	0.4639	0.7861
1	-1.09648	-0.46526	0.6356	0.4660	0.7881
1.1	-1.10055	-0.45326	0.6381	0.4732	0.7944
1.2	-1.10031	-0.45730	0.6386	0.4881	0.8038
1.3	-1.09232	-0.43877	0.6351	0.4983	0.8073
1.4	-1.09489	-0.46230	0.6332	0.5018	0.8079
1.5	-1.09624	-0.48630	0.6350	0.5020	0.8095
1.6	-1.06842	-0.43494	0.6329	0.4991	0.8060
1.7	-1.05450	-0.42730	0.6311	0.4926	0.8006
1.8	-1.04062	-0.38984	0.6285	0.4894	0.7966
1.9	-1.01363	-0.34684	0.6225	0.4909	0.7928
2	-1.01486	-0.33529	0.6215	0.4901	0.7915
2.2	-1.00680	-0.31727	0.6220	0.4905	0.7921
2.4	-0.97869	-0.27922	0.6149	0.4993	0.7921
2.6	-0.96311	-0.28332	0.6120	0.4946	0.7869
2.8	-0.97257	-0.29193	0.6135	0.4752	0.7760
3	-0.95680	-0.27752	0.6162	0.4621	0.7702
3.2	-0.90714	-0.26346	0.6061	0.4731	0.7689
3.4	-0.96799	-0.31569	0.6042	0.4643	0.7620
3.6	-0.93492	-0.20615	0.5989	0.4699	0.7612
3.8	-0.68092	0.00000	0.6353	0.5279	0.8260
4	-0.84083	0.00000	0.6230	0.5082	0.8040

V_{CON} = 1000 m/s and V_{REF}= 600 m/s. c=2.5g and n=3.2.

FIGURES

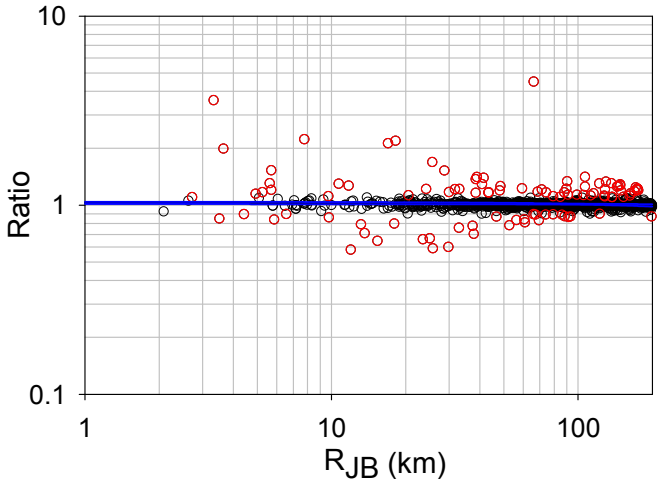

Figure 1. Comparisons of the R_{JB} values obtained from the first and second plane solutions. There are 1773 data points on the plot. Red circles represent the data having ratios either less than 0.9 or greater than 1.1. Black line shows the mean estimations and blue lines show the 95% confidence intervals of the mean trend line.

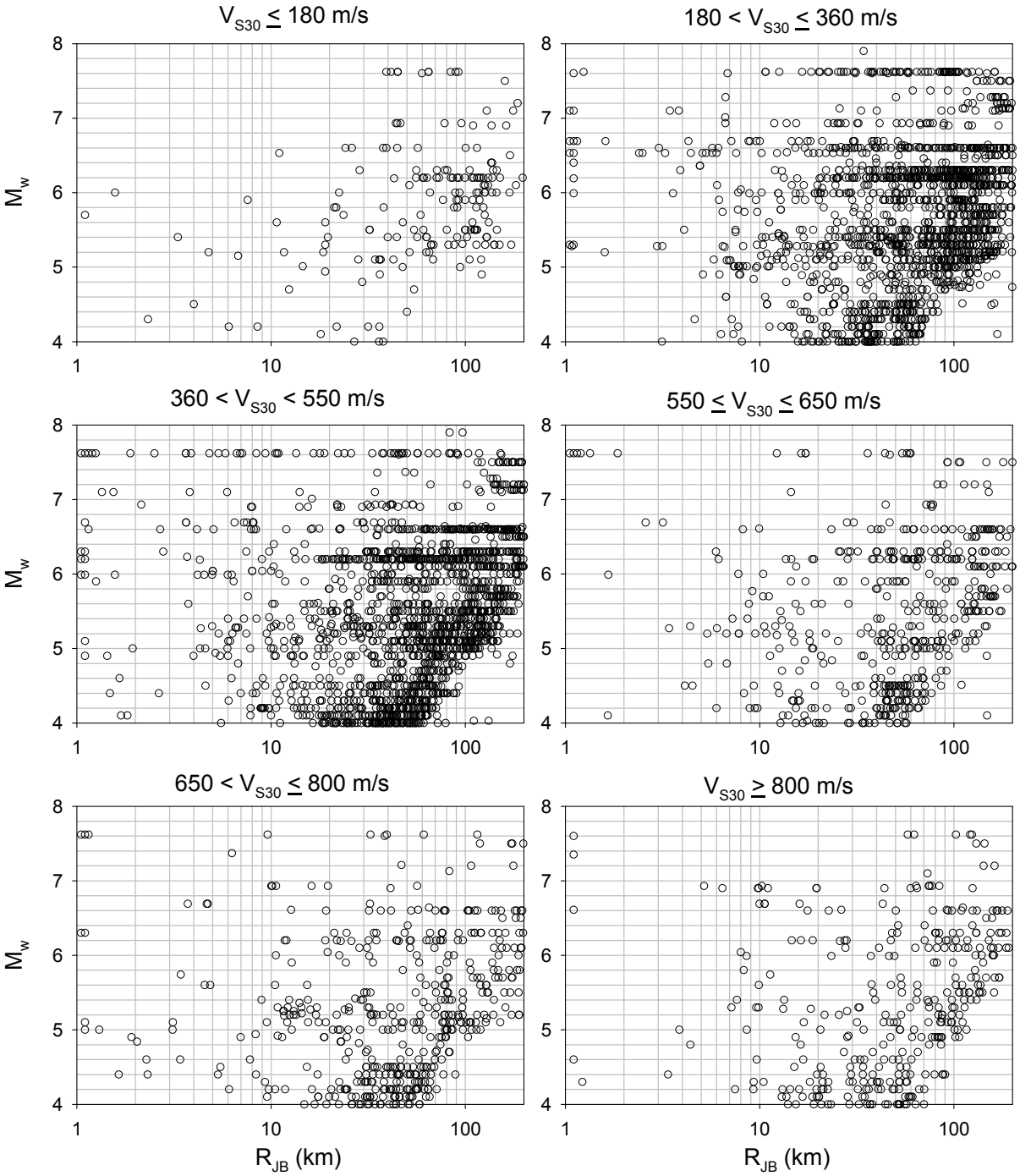

Figure 2. R_{JB} vs. M_w scatters of the database for different V_{S30} bins.

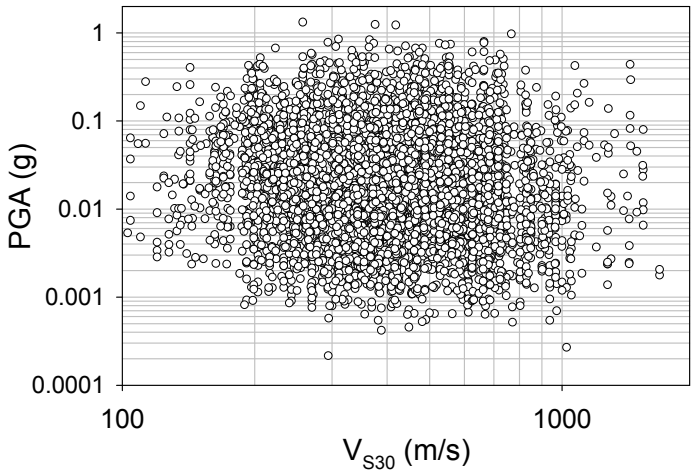

Figure 3. V_{S30} vs. PGA scatters of the database.

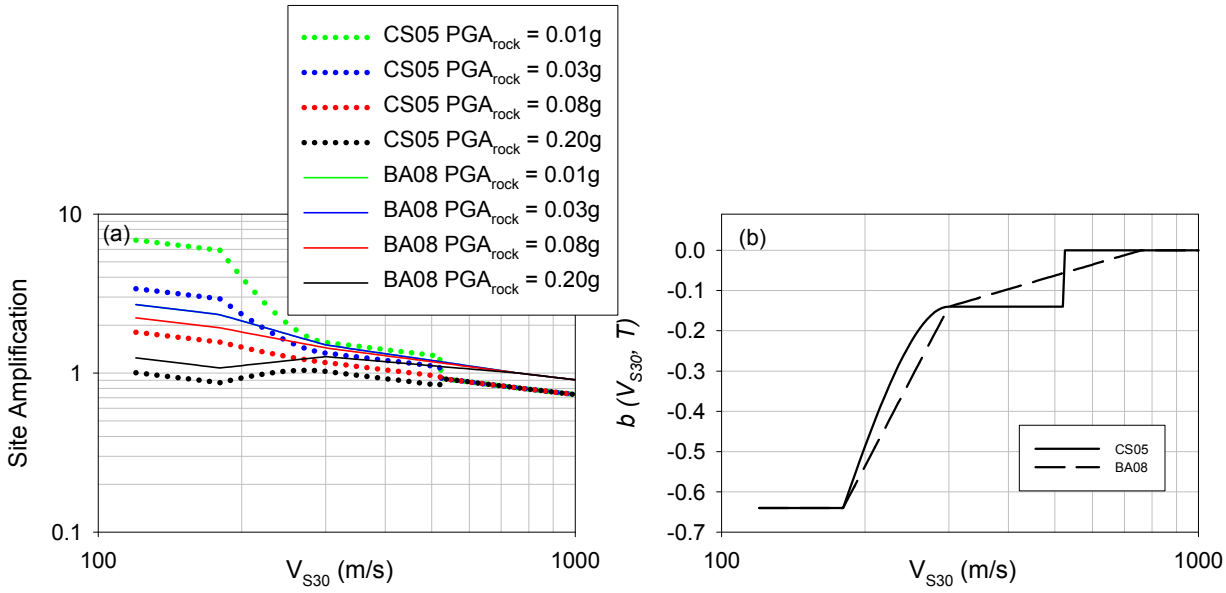

Figure 4. (a) Comparisons between the amplification factors derived from Choi and Stewart (2005), [CS05] and Boore and Atkinson (2008), [BA08] for PGA. Each line represents different levels of input rock motion. (b) Comparison of the nonlinear coefficients for T = 0.0 s proposed by CS05 and BA08.

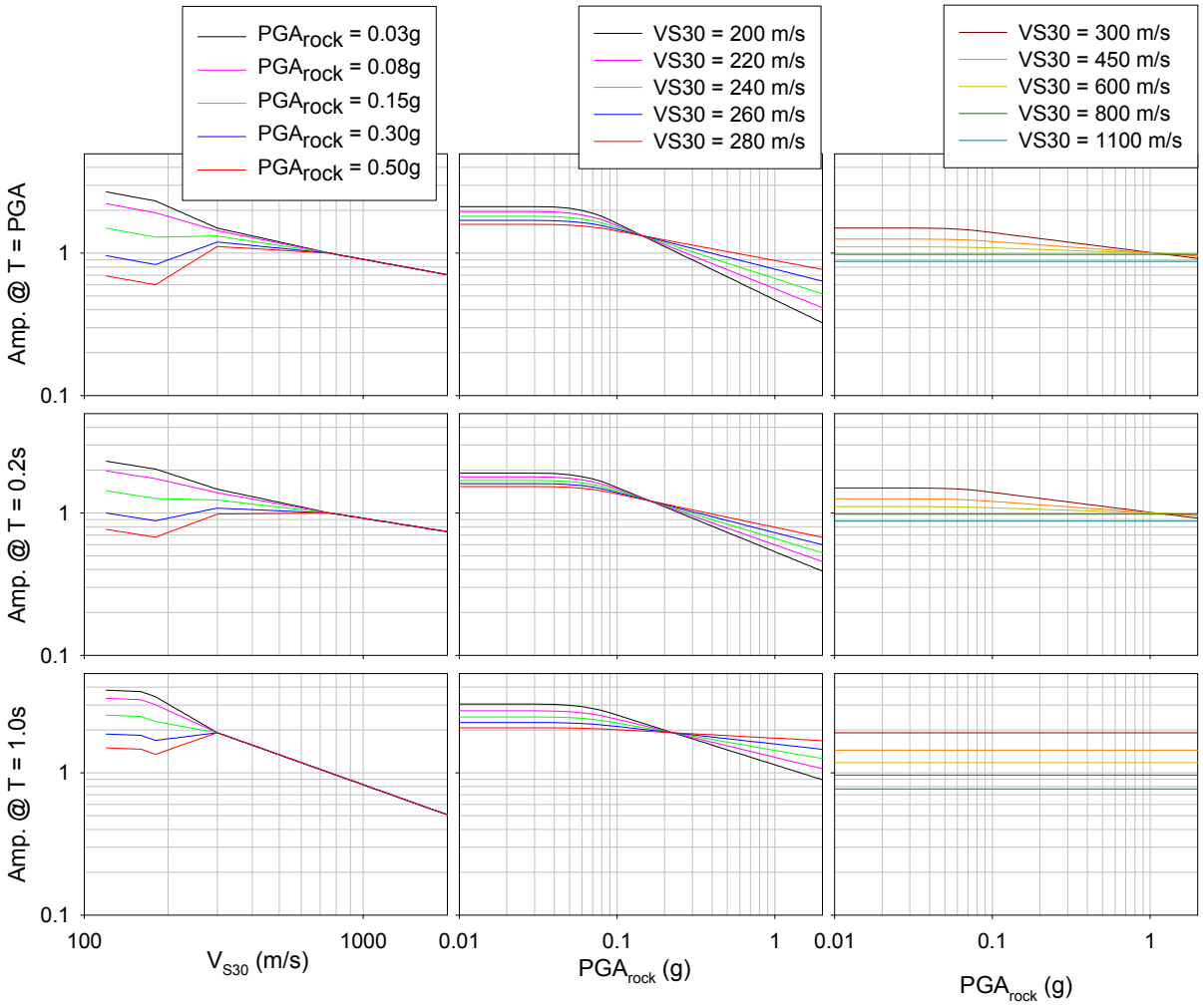

Figure 5. Site amplifications proposed by Boore and Atkinson (2008) for T = 0.0 s, 0.2 s and 1.0 s. The left column shows the variation of the site amplification with respect to V_{S30} for different levels of PGA_{rock}. The middle and right columns show the variation of the site amplifications as a function of PGA_{rock} for different V_{S30} values (V_{S30} ranges between 200m/s and 280m/s in the middle column plots whereas V_{S30} changes from 300m/s to 1100m/s in the right column plots).

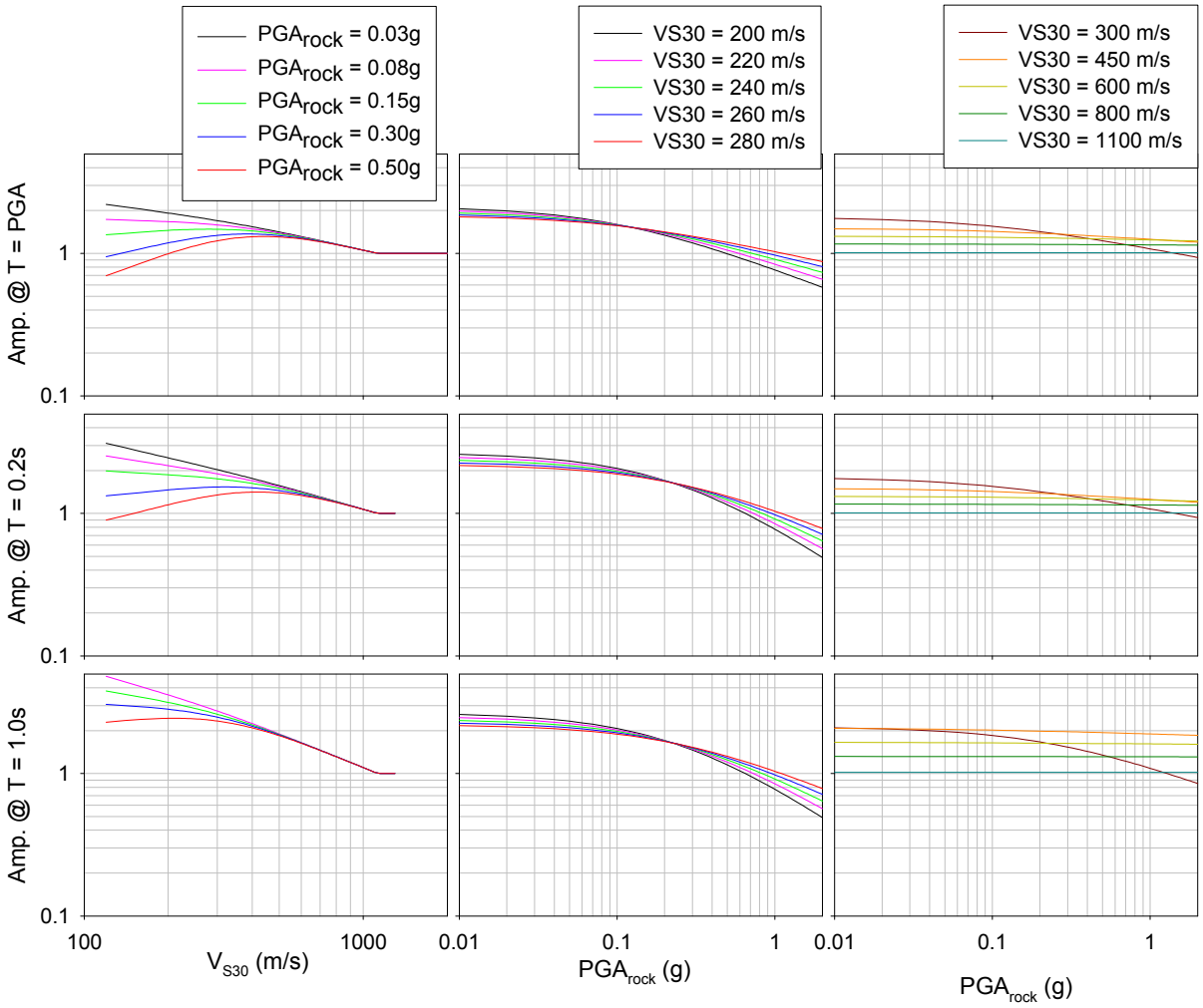

Figure 6. Same as Figure 5 but for CY08.

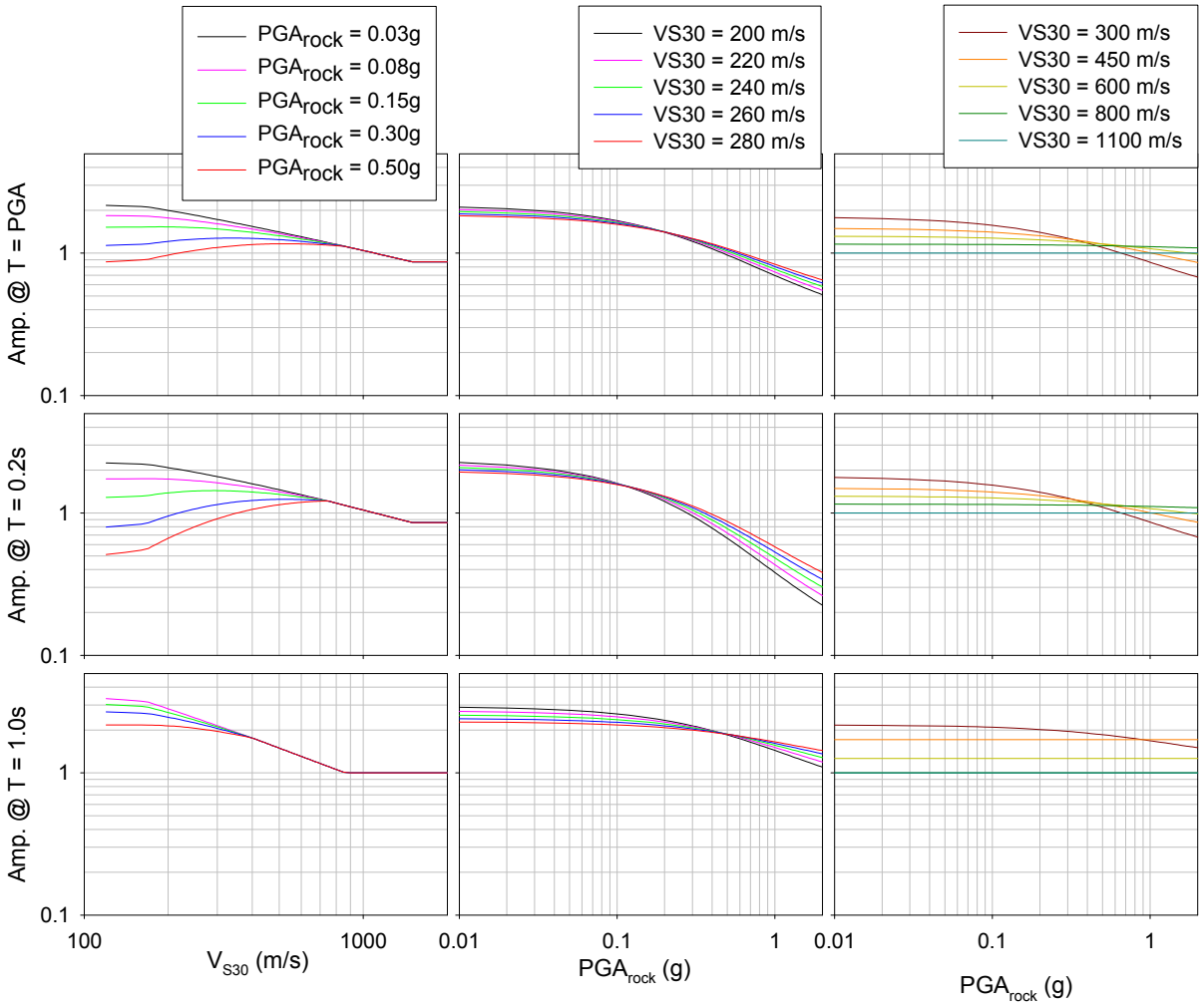

Figure 7. Same as Figure 5 but for AS08.

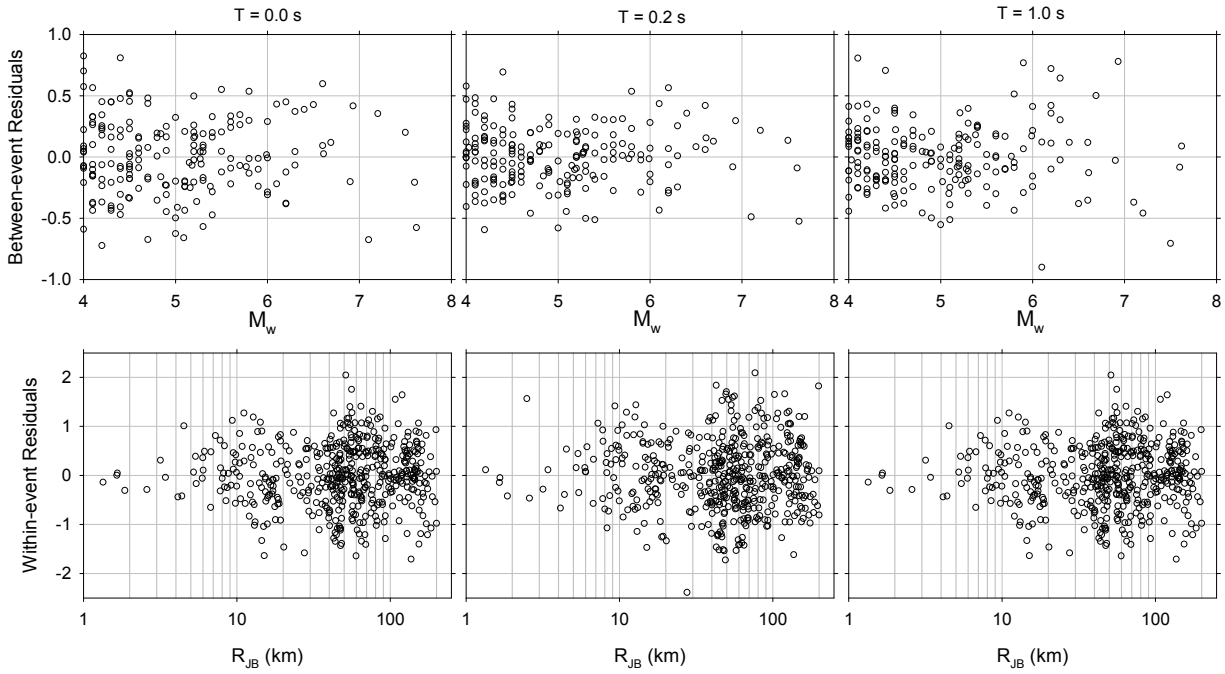

Figure 8. Between- and within-event residual scatters of the GMPE that is used for calculating the reference rock motion at V_{S30} = 600 m/s. The top row illustrates the variations in terms of M_w and the bottom row shows the residual distributions as a function of R_{JB}. Left, middle and right columns display the results for T = 0.0 s, T=0.2 s, and T=1.0 s, respectively.

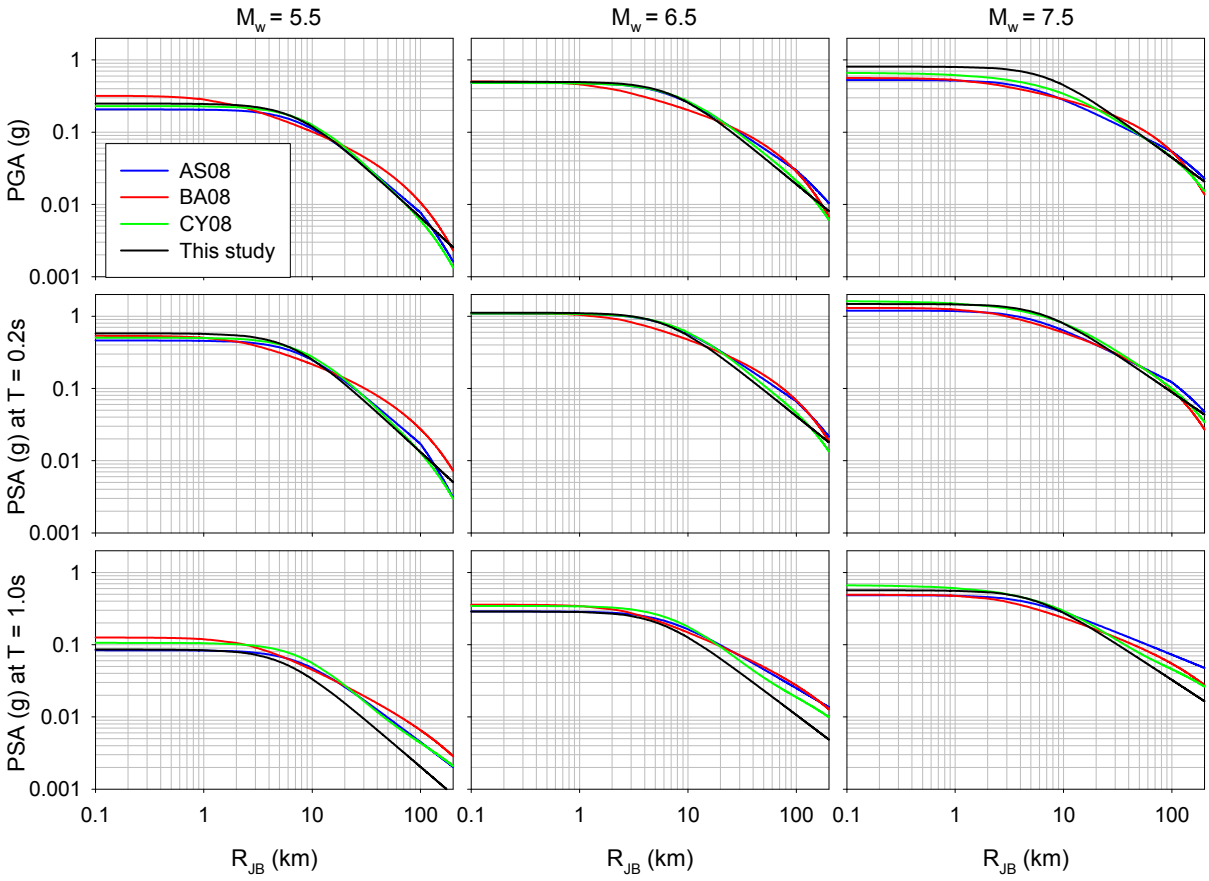

Figure 9.The comparison of the proposed rock estimations with 3 NGA GMPEs (Abrahamson and Silva, 2008 [AS08], Boore and Atkinson, 2008 [BA08] and Chiou and Youngs, 2008 [CY08]) at V_{S30} = 600 m/s. The left, middle, and right column illustrate variation in M_w = 5.5, M_w = 6.5, M_w = 7.5, respectively. Top, middle and bottoms rows successively show the variation of the intensity measure for T = 0.0 s, T=0.2 s, and T=1.0 s.

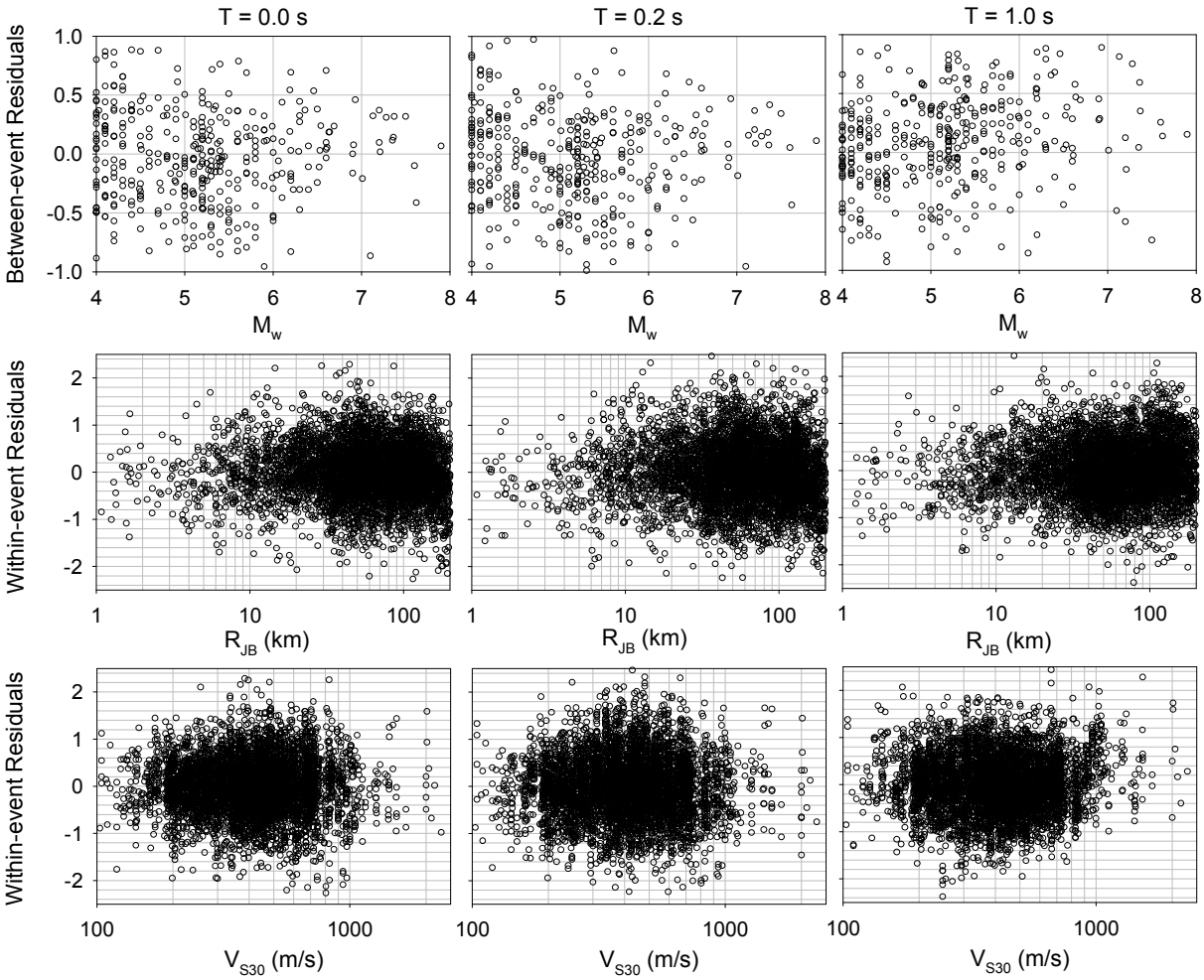

Figure 10. Between- and within-event residual distribution of the proposed site model. Left, middle and right columns show the distribution for T = 0.0 s, T = 0.2 s, and T = 1.0 s, respectively.

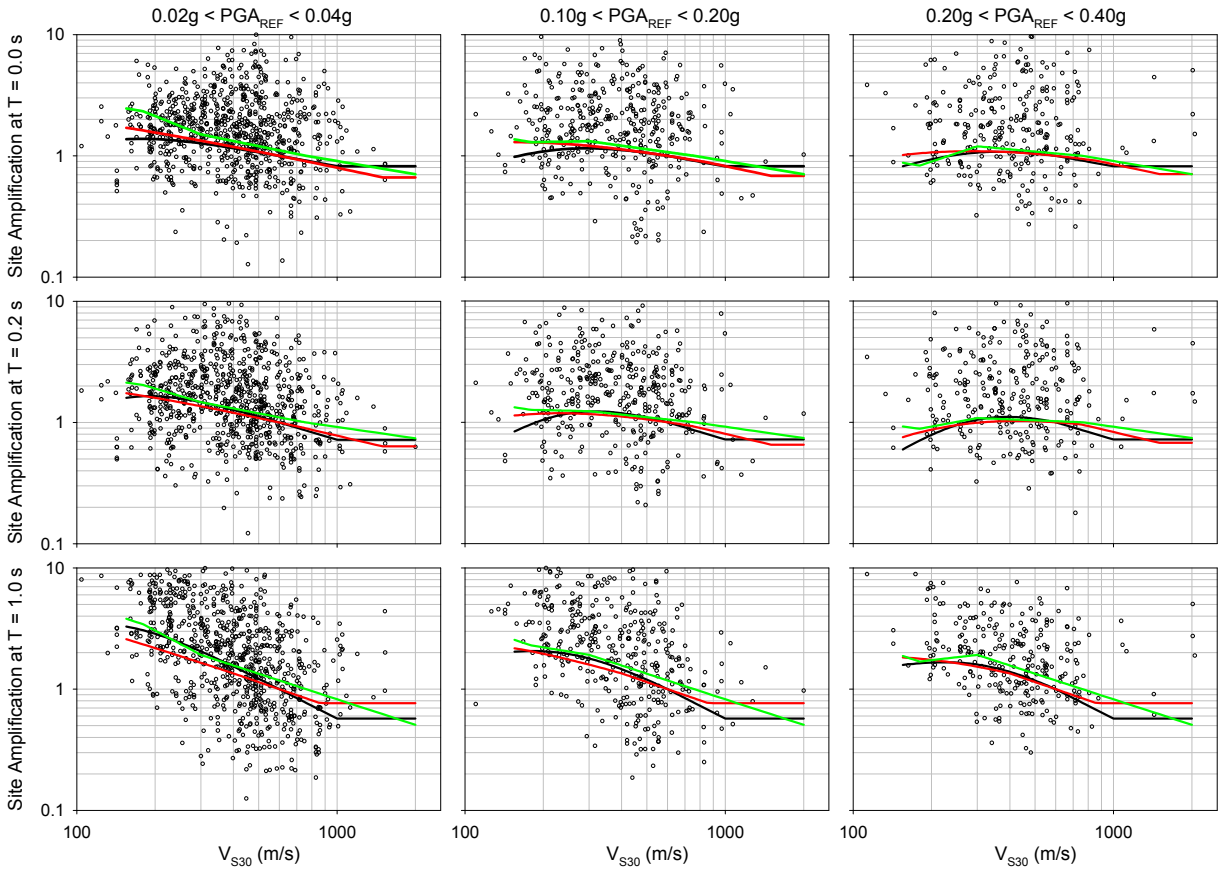

Figure 11. Comparisons of the proposed site model (black curve) with AS08 (red curve) and BA08 (green curve) together with the empirical data for T = 0.0 s, T = 0.2 s, and T = 1.0 s (from top to bottom respectively). Each column represents different level of input rock motion, PGA_{REF} indicated at the top of figure.

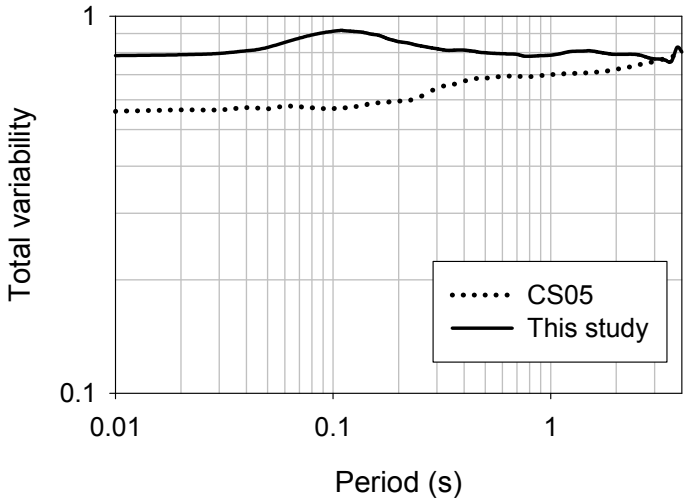

Figure 12. Comparison of the total variability of the proposed site model (solid line) with CS05 site model (dashed line).